

## Effect of Zr Content on Microstructure and Oxidation Resistance of Nb-Ti-Si-Based Ultrahigh Temperature Alloys (Postprint)

**Authors:** Zeng Yuxiang, Guo Xiping, Qiao Yanqiang, Zhongyi Nie

**Date:** 2023-03-19T00:00:00+00:00

### Abstract

Nb- Ti- Si base in situ composites which consist of Nb solid solution (Nbss) and silicides (a-Nb<sub>5</sub>Si<sub>3</sub>, b-Nb<sub>5</sub>Si<sub>3</sub>, g-Nb<sub>5</sub>Si<sub>3</sub> and/or Nb<sub>3</sub>Si) phases, have shown great potential as alternative materials to Ni-based superalloys due to their high melting points (beyond 1700 °C ), good formability, low density (6.6~7.2 g/cm<sup>3</sup>) and high strength. However, a major hindrance to the applications of these alloys at elevated temperatures is their poor oxidation resistance. Alloying is an effective method to improve the integrated properties of the alloys, especially for the oxidation resistance. Up to now, many beneficial elements such as Ti, Al, Cr and Sn have been employed to ameliorate their oxidation resistance. Nevertheless, there is no systematic and comprehensive investigation on the effect of Zr contents on the microstructure and oxidation behavior of the alloys based on Nb-Ti-Si system. The aim of this work is to clarify the effects of Zr contents on phase selection, microstructure and high temperature oxidation resistance of Nb-Ti-Si based alloys in detail. The constituent phases, microstructure and composition of the alloys under as-cast state and after oxidation were investigated by OM, XRD, SEM and EDS. Thus, six Nb-Ti- Si base ultrahigh-temperature alloys with compositions of Nb-22Ti-15Si-5Cr-3Hf-3Al-xZr (x=0, 0.5, 1, 2, 4, 8, atomic fraction, %) were prepared by vacuum non-consumable arc-melting. The results show that the alloys with different Zr contents are mainly composed of Nbss and g-(Nb, X)<sub>5</sub>Si<sub>3</sub> (X represents Ti, Hf, Cr and Zr). However, the addition of Zr has an obvious affect on the microstructure of Nb-Ti-Si base alloys. Both the sizes and amounts of primary g- (Nb, X)<sub>5</sub>Si<sub>3</sub> increase with increase in Zr contents. Alloys with different Zr contents were oxidized at 1250 °C for 1~50 h, respectively. It is found that both adhesion and compactness of the scales are improved effectively by increase in Zr contents. The scales of alloys with higher Zr contents (x=4 and 8) after oxidation for 50 h show an obvious layered structure: the outmost layer is only composed of TiO<sub>2</sub>, the middle layer mainly consists of ZrO<sub>2</sub>, TiNb<sub>2</sub>O<sub>7</sub> and TiO<sub>2</sub>, and the inner layer is mainly comprised of

Si-rich oxides. The mass gain per unit area and the thickness of the scale after oxidation decrease with increase in Zr contents in the alloys, indicating that the addition of Zr can improve the oxidation resistance of the alloys significantly.

## Full Text

# EFFECT OF Zr ADDITION ON MICROSTRUCTURE AND OXIDATION RESISTANCE OF Nb-Ti-Si BASE ULTRAHIGH-TEMPERATURE ALLOYS

Yuxiang Zeng<sup>1</sup>, Xiping Guo<sup>1</sup>, Yanqiang Qiao<sup>1</sup>, Zhongyi Nie<sup>2</sup>

<sup>1</sup> State Key Laboratory of Solidification Processing, Northwestern Polytechnical University, Xi'an 710072, China

<sup>2</sup> Sinosteel Xi'an Heavy Machinery Co. Ltd., Xi'an 710077, China

**Correspondent:** Xiping Guo, professor, Tel: (029)88494873, E-mail: xpguo@nwpu.edu.cn

---

## Abstract

Nb-Ti-Si base in situ composites consisting of Nb solid solution (Nbss) and silicides ( $\alpha$ -Nb<sub>5</sub>Si<sub>3</sub>,  $\beta$ -Nb<sub>5</sub>Si<sub>3</sub>,  $\gamma$ -Nb<sub>5</sub>Si<sub>3</sub> and/or Nb<sub>3</sub>Si) phases have shown great potential as alternative materials to Ni-based superalloys due to their high melting points (beyond 1700 °C), good formability, low density (6.6–7.2 g/cm<sup>3</sup>), and high strength. However, a major hindrance to their elevated-temperature applications is poor oxidation resistance. Alloying is an effective method to improve the integrated properties of these alloys, particularly oxidation resistance. To date, many beneficial elements such as Ti, Al, Cr, and Sn have been employed to ameliorate their oxidation behavior. Nevertheless, no systematic and comprehensive investigation has been conducted on the effect of Zr content on the microstructure and oxidation behavior of Nb-Ti-Si based alloys. This work aims to clarify in detail the effects of Zr content on phase selection, microstructure, and high-temperature oxidation resistance of Nb-Ti-Si based alloys.

Six Nb-Ti-Si base ultrahigh-temperature alloys with compositions of Nb-22Ti-15Si-5Cr-3Hf-3Al-xZr ( $x = 0, 0.5, 1, 2, 4, 8$ , atomic fraction, %) were prepared by vacuum non-consumable arc-melting. The constituent phases, microstructure, and composition of the alloys in the as-cast state and after oxidation were investigated using optical microscopy (OM), X-ray diffraction (XRD), scanning electron microscopy (SEM), and energy-dispersive spectroscopy (EDS). The results show that all alloys with different Zr contents are mainly composed of Nbss and  $\gamma$ -(Nb, X)<sub>5</sub>Si<sub>3</sub> (X represents Ti, Hf, Cr, and Zr). However, Zr addition has an obvious effect on the microstructure of Nb-Ti-Si base alloys: both the size and amount of primary  $\gamma$ -(Nb, X)<sub>5</sub>Si<sub>3</sub> increase with increasing Zr content. Alloys with different Zr contents were oxidized at 1250 °C for 1–50 h. It was found

that both the adhesion and compactness of the scales are effectively improved by increasing Zr content. The scales of alloys with higher Zr contents ( $x = 4$  and  $8$ ) after oxidation for 50 h show an obvious layered structure: the outmost layer is composed only of  $\text{TiO}_2$ , the middle layer mainly consists of  $\text{ZrO}_2$ ,  $\text{TiNb}_2\text{O}_7$ , and  $\text{TiO}_2$ , and the inner layer is mainly comprised of Si-rich oxides. The mass gain per unit area and the thickness of the scale after oxidation decrease with increasing Zr content in the alloys, indicating that Zr addition can significantly improve oxidation resistance.

**KEY WORDS** Nb-Ti-Si base ultrahigh-temperature alloy, phase constituent, microstructure, high-temperature oxidation

---

## Introduction

With the rapid development of aerospace technology, hot-end structural materials are required to operate at temperatures above  $1150\text{ }^\circ\text{C}$ . Traditional Ni-based single-crystal superalloys can no longer meet these service requirements due to their melting point limitations, making the research of new-generation high-temperature structural materials to replace Ni-based single-crystal superalloys imperative [1–3]. Nb-Ti-Si base ultrahigh-temperature alloys have become one of the most promising candidate materials due to their high melting points, low density, high-temperature strength, and good creep resistance [3–6]. However, Nb-Ti-Si base ultrahigh-temperature alloys suffer from poor oxidation resistance and are prone to peeling oxidation, which represents a major obstacle to their development and application [1–3,7].

Alloying can effectively improve the oxidation resistance of Nb-Ti-Si base ultrahigh-temperature alloys [1–3,7–10]. Currently, common alloying elements that can improve the high-temperature oxidation resistance of this alloy system include Al, B, Cr, and Sn [8]. Wang et al. [7] and Zhang and Guo [8] found that the alloying element B has a significant effect on improving the high-temperature oxidation resistance of Nb-Ti-Si base ultrahigh-temperature alloys. References [11–15] indicate that adding an appropriate amount of Cr can promote the formation of the Laves phase  $\text{Cr}_2\text{Nb}$ , thereby improving oxidation resistance. Adding Sn can effectively suppress peeling oxidation of Nb-Si base alloys at intermediate temperatures [16–19].

Zr, as a high-melting-point and active element, is a common alloying element in high-temperature structural materials. In Al-Mg-Si alloys, Zr addition can significantly refine the grain structure, reduce the size of primary dendrites, and promote more uniform distribution of fine intermetallic compounds [20]. Zr also has beneficial alloying effects in Mo-Si-B base ultrahigh-temperature alloys, promoting rapid formation of protective oxide scales during oxidation and thereby effectively improving oxidation resistance [21,22]. Furthermore, Zr oxide ( $\text{ZrO}_2$ ) is a primary raw material for thermal barrier coatings on high-temperature alloy blades [23].

In recent years, studies [24,25] have used Zr to modify silicide coatings on Nb-Ti-Si base ultrahigh-temperature alloys, finding that after oxidation at 1250 °C for 100 h, a dense and complete mixed oxide scale composed of  $\text{TiO}_2$  and  $\text{SiO}_2$  (containing a small amount of  $\text{ZrO}_2$  particles) formed, which could effectively protect the alloy. Tian et al. [26] investigated the effect of Zr content in Nb-Ti-Si base alloys and found that the hardness of both Nbss and silicides increased with Zr content, while the room-temperature yield strength showed a linear increasing relationship with Zr content, and the room-temperature fracture toughness first increased and then decreased with increasing Zr content. However, the alloying effect of Zr in Nb-Ti-Si base ultrahigh-temperature alloys has not been fully understood, particularly regarding high-temperature oxidation behavior. Therefore, this work systematically investigates the influence of Zr content on the microstructure and high-temperature oxidation resistance of Nb-Ti-Si base ultrahigh-temperature alloys.

---

## 1. Experimental Methods

High-purity Nb blocks, Si blocks, Cr blocks, Al blocks, primary sponge Ti, and high-purity Zr particles were used to prepare six alloy ingots (200 g each) with different Zr contents. The alloy compositions were Nb-22Ti-15Si-5Cr-3Hf-3Al-xZr ( $x = 0, 0.5, 1, 2, 4, 8$ , atomic fraction, %). For convenience, these six alloys are denoted as xZr ( $x = 0, 0.5, 1, 2, 4, 8$ ). The raw materials were acid-washed or alkali-washed, then rinsed with pure water, dried, weighed according to the proportions, and melted in a water-cooled Cu crucible in a custom vacuum non-consumable arc-melting furnace. Each alloy ingot was remelted six times with electromagnetic stirring applied during the final stage of each melting to ensure compositional homogeneity.

Using electrical discharge machining, 8 mm × 8 mm × 8 mm cubic specimens were cut from the same location of each button ingot for as-cast microstructure analysis and isothermal oxidation testing. The specimen surfaces were ground stepwise with SiC waterproof abrasive paper, then ultrasonically cleaned in ethanol, dried, weighed, and measured for surface area. Static oxidation was conducted in a custom high-temperature oxidation furnace at 1250 °C for 1, 5, 10, 20, and 50 h, after which the oxidation mass gain was measured upon furnace cooling.

The oxide scale thickness was measured at 20 different locations using a PM-G3 optical microscope (OM) and averaged. The microstructure, composition, and phase constituents of the as-cast specimens and oxidized samples were characterized using an X Pert PRO X-ray diffractometer (XRD) and a MIRA 3 scanning electron microscope (SEM) equipped with an energy-dispersive spectrometer (EDS). Backscattered electron (BSE) imaging was performed at an accelerating voltage of 20 kV and a current of 12 mA.

## 2. Results and Discussion

### 2.1 Phase Composition and Microstructure

Figure 1 [Figure 1: see original paper] shows the XRD spectra of the six Nb-Ti-Si base alloys with different Zr contents in the as-cast state, and Table 1 presents the EDS analysis results of the phase compositions. All six alloys consist of Nbss and  $\gamma$ -(Nb, X)<sub>5</sub>Si<sub>3</sub> (where X is Ti, Hf, Cr, and Zr) phases, with no  $\alpha$ -(Nb, X)<sub>5</sub>Si<sub>3</sub> or  $\beta$ -(Nb, X)<sub>5</sub>Si<sub>3</sub> detected. This is because both Hf<sub>5</sub>Si<sub>3</sub> and Zr<sub>5</sub>Si<sub>3</sub> have a hexagonal D88 crystal structure, identical to that of  $\gamma$ -(Nb, X)<sub>5</sub>Si<sub>3</sub> [26]; therefore, Hf and Zr additions favor the formation of  $\gamma$ -(Nb, X)<sub>5</sub>Si<sub>3</sub>. EDS analysis reveals that in the 8Zr alloy, the Zr content in the  $\gamma$ -(Nb, X)<sub>5</sub>Si<sub>3</sub> phase is as high as 15.5%, while the Zr content in the Nbss phase is only 2.2% (Table 1). Zr preferentially dissolves in the  $\gamma$ -(Nb, X)<sub>5</sub>Si<sub>3</sub> phase, substituting for Nb atoms.

Figure 2 [Figure 2: see original paper] shows BSE images of the as-cast microstructures of the six alloys with different Zr contents. The 0Zr and 0.5Zr alloys exhibit near-eutectic microstructures, with the typical Nbss/ $\gamma$ -(Nb, X)<sub>5</sub>Si<sub>3</sub> eutectic structure occupying more than 90% of the area fraction and displaying a fine, petal-like morphology. When the Zr content increases to 1% and 2%, the eutectic structure fraction decreases to approximately 86% and 82%, respectively. In the 4Zr and 8Zr alloys, the eutectic structure content is only about 75% and 73%, respectively, indicating that increasing Zr content in Nb-Ti-Si base ultrahigh-temperature alloys shifts the eutectic point toward lower Si content.

Furthermore, both the content and morphology of primary  $\gamma$ -(Nb, X)<sub>5</sub>Si<sub>3</sub> change significantly with increasing Zr content, as shown in Figure 2. In the 0Zr and 0.5Zr alloys, the primary  $\gamma$ -(Nb, X)<sub>5</sub>Si<sub>3</sub> content is relatively low, with sizes mostly between 25–100 nm, distributed between the Nbss/ $\gamma$ -(Nb, X)<sub>5</sub>Si<sub>3</sub> eutectic colonies. In the 1Zr and 2Zr alloys, the primary  $\gamma$ -(Nb, X)<sub>5</sub>Si<sub>3</sub> appears as elongated plate-like structures with sizes of approximately 30–180 nm. In the 4Zr and 8Zr alloys, the primary  $\gamma$ -(Nb, X)<sub>5</sub>Si<sub>3</sub> exhibits a typical hexagonal morphology with sizes ranging from 60–270 nm. In all six alloys, a dark-contrast structure exists between Nbss dendrites (Figure 2e). Based on combined EDS and SEM analysis, this structure is identified as a three-phase low-melting-point eutectic. Li and Guo [27] observed a similar three-phase eutectic structure in the mushy zone cross-section of directionally solidified Nb-Ti-Si base alloys, which was identified by EDS as Cr<sub>2</sub>Nb/Nbss/ $\gamma$ -(Nb, X)<sub>5</sub>Si<sub>3</sub>.

### 2.2 Oxidation Behavior

**2.2.1 Oxidation Kinetics** Oxidation time-mass gain curves and oxidation time-scale thickness curves are commonly used to characterize oxidation kinetics. Figure 3 [Figure 3: see original paper] shows the oxidation time-mass gain kinetics curves for alloys with different Zr contents after static oxidation at 1250 °C. The oxidation kinetics curves for all six alloys at 1250 °C are approximately

parabolic. Since the oxidation behavior of 0Zr and 0.5Zr alloys, 1Zr and 2Zr alloys, and 4Zr and 8Zr alloys are respectively similar, the following analysis will focus on the 0Zr, 2Zr, and 8Zr alloys as representative examples.

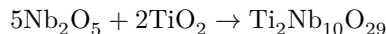
When the oxidation time is less than 10 h, the mass gain behavior of all six alloys is similar. Compared with the 0Zr alloy, the 8Zr alloy with higher Zr content shows a slight decrease in mass gain, indicating that Zr addition and increased Zr content do not significantly improve the short-term oxidation performance of Nb-Ti-Si base ultrahigh-temperature alloys. However, when the oxidation time extends to 20 h, the mass gains of the 0Zr, 2Zr, and 8Zr alloys are 62.71, 55.23, and 46.34 mg/cm<sup>2</sup>, respectively, demonstrating that increased Zr content has a more obvious effect on improving oxidation resistance during longer oxidation periods. Particularly when the oxidation time extends to 50 h, the mass gain of the 0Zr alloy is 94.99 mg/cm<sup>2</sup>, while that of the 8Zr alloy is only 58.03 mg/cm<sup>2</sup>—approximately 60% of the 0Zr alloy's mass gain. This indicates that increased Zr content can significantly improve the long-term oxidation resistance of Nb-Ti-Si base ultrahigh-temperature alloys.

Furthermore, the parabolic rate constants for the oxidation time-mass gain per unit area curves of the 0Zr, 0.5Zr, 1Zr, 2Zr, 4Zr, and 8Zr alloys oxidized at 1250 °C are 89.9, 85.4, 83.9, 82.2, 57.7, and 59.2 mg<sup>2</sup>/(cm<sup>4</sup> · s), respectively. These results demonstrate that the oxidation resistance of Nb-Ti-Si base ultrahigh-temperature alloys improves significantly with increasing Zr content, with the 4Zr and 8Zr alloys exhibiting better oxidation performance.

### 2.2.2 Macroscopic Morphology and Microstructure of Oxide Scales

After oxidation at 1250 °C for 1 h, the oxide scales on all Zr-containing alloys spalled and fractured. After 5 h, powdery material could be observed near the spalled oxide scales due to the porous inner layer. With extended oxidation time (10 and 20 h), the spalled outer oxide scales became more compact, with no powdery material present. After 50 h (Figure 4 [Figure 4: see original paper]), scale spalling occurred only on the 0Zr, 0.5Zr, 1Zr, and 2Zr alloys, while the oxide scales on the 4Zr and 8Zr alloys remained well-bonded to the substrate without spalling.

The oxide scales were ground into powder for XRD analysis, with results shown in Figure 5 [Figure 5: see original paper]. Combined with EDS analysis, after oxidation at 1250 °C for 1, 5, 10, and 20 h, all alloys with different Zr contents show similar phase constituents in their oxide scales, primarily consisting of TiNb<sub>2</sub>O<sub>7</sub>, Ti<sub>2</sub>Nb<sub>10</sub>O<sub>29</sub>, TiO<sub>2</sub>, and Nb<sub>2</sub>O<sub>5</sub>. Ti<sub>2</sub>Nb<sub>10</sub>O<sub>29</sub> is a metastable intermediate phase that tends to transform to TiNb<sub>2</sub>O<sub>7</sub> with prolonged oxidation time according to the reaction [10]:



Figures 6a, 6c, and 6e [Figure 6: see original paper] show BSE images of cross-sections of the outer oxide scales formed on the 0Zr, 2Zr, and 8Zr alloys after oxidation at 1250 °C for 5 h. The oxide scale structures and phase compositions of the three alloys are similar after 5 h oxidation, with thicknesses of 26.5, 24.4, and 21.1  $\mu\text{m}$ , respectively. The scale thickness shows only a slight decrease with increasing Zr content, indicating that Zr content does not significantly improve the oxidation resistance of Nb-Ti-Si base ultrahigh-temperature alloys during short oxidation times. However, numerous relatively large pores exist in the oxide scales of the 0Zr and 2Zr alloys, while the 8Zr alloy scale contains fewer and smaller pores. This demonstrates that Zr addition indeed improves scale compactness. The reason may be that the oxide scale of the 0Zr alloy consists mainly of porous  $\text{Ti}_2\text{Nb}_{10}\text{O}_{29}$  phase, while the 2Zr alloy scale contains both porous  $\text{Ti}_2\text{Nb}_{10}\text{O}_{29}$  and compact  $\text{TiNb}_2\text{O}_7$  phases, and the 8Zr alloy scale consists mainly of compact  $\text{TiNb}_2\text{O}_7$  phase. This indicates that Zr addition promotes the reactions shown in equations (1) and (2) during oxidation, thereby improving scale compactness.

Figures 6b, 6d, and 6f [Figure 6: see original paper] show BSE images of the internal oxidation zones of the 0Zr, 2Zr, and 8Zr alloys after oxidation at 1250 °C for 5 h. The oxidation products in the internal oxidation zones of the three alloys are similar, where the dark black phase is  $\text{TiO}_2$  and the white needle-like or rod-like phase is  $\text{HfO}_2$ , because Ti and Hf have strong affinity for oxygen and are preferentially oxidized. EDS analysis of the internal oxidation zones of the 0Zr, 2Zr, and 8Zr alloys (Table 2) shows that the O content in Nbss and  $\gamma\text{-(Nb, X)}_5\text{Si}_3$  is higher in the 0Zr alloy but lower in the 8Zr alloy, indicating that the internal oxidation degree is lower in alloys with higher Zr content.

Figure 7 [Figure 7: see original paper] shows the XRD spectra of the oxide scales on the 0Zr, 2Zr, and 8Zr alloys after oxidation at 1250 °C for 50 h. Combined with EDS analysis, the phase compositions of the oxide scales on the 0Zr and 2Zr alloys are similar, mainly consisting of  $\text{TiNb}_2\text{O}_7$ ,  $\text{Ti}_2\text{Nb}_{10}\text{O}_{29}$ ,  $\text{TiO}_2$ , and  $\text{Nb}_2\text{O}_5$ , while  $\text{ZrO}_2$  appears in the oxide scale of the 8Zr alloy. Quantitative metallographic analysis reveals that the content of each oxide changes with increasing Zr content in the alloys. From BSE images of cross-sections of the oxide scales on these three alloys (Figure 8 [Figure 8: see original paper]),  $\text{ZrO}_2$  appears as white rod-like or granular particles (arrow 7) approximately 3–5  $\mu\text{m}$  in size, distributed at the interfaces between compact  $\text{TiO}_2$  (arrow 6) and  $\text{TiNb}_2\text{O}_7$  (arrow 8) phases, but rarely as large blocks or networks.

The oxide scale thicknesses of the 0Zr and 2Zr alloys are approximately 589 and 554  $\mu\text{m}$ , respectively, showing no significant difference, while that of the 8Zr alloy is 393  $\mu\text{m}$ —substantially thinner than the 0Zr and 2Zr alloys. This indicates that the 8Zr alloy exhibits significantly better oxidation resistance. Moreover, the oxide scale of the 0Zr alloy shows obvious cracks parallel to the scale-substrate interface and contains some relatively large pores. The 2Zr alloy scale contains no large cracks but still has pores, while the 8Zr alloy scale is very compact with almost no pores (Figure 8). The presence of numerous cracks

and pores in the oxide scales of the 0Zr and 2Zr alloys may be due to the formation of substantial  $\text{Nb}_2\text{O}_5$  and  $\text{Ti}_2\text{Nb}_{10}\text{O}_{29}$  during oxidation. Research [28] has shown that  $\text{Nb}_2\text{O}_5$  is a non-protective oxide with a Pilling-Bedworth Ratio (PBR) of approximately 2.68. The presence of  $\text{Nb}_2\text{O}_5$  in the oxide scale generates large volume expansion, causing internal stresses in the scale to exceed the scale-substrate bonding strength, leading to scale cracking and spalling. Higher Zr content accelerates the reactions shown in equations (1) and (2), suppressing  $\text{Nb}_2\text{O}_5$  and  $\text{Ti}_2\text{Nb}_{10}\text{O}_{29}$  formation while promoting  $\text{TiO}_2$  and  $\text{TiNb}_2\text{O}_7$  generation, thereby effectively improving the compactness of the oxide scale formed on the alloy surface.

As shown in Figure 8, the oxide scales of the 0Zr and 2Zr alloys exhibit a single-layer structure, while that of the 8Zr alloy clearly shows a multilayer structure. The outermost layer of the 8Zr alloy scale is approximately 25  $\mu\text{m}$  thick. XRD and EDS analyses of this layer (Figure 7 and Table 3) identify it as  $\text{TiO}_2$ . The middle layer is approximately 280–300  $\mu\text{m}$  thick and consists mainly of  $\text{TiNb}_2\text{O}_7$ ,  $\text{TiO}_2$ , and  $\text{ZrO}_2$ . The inner layer is about 65  $\mu\text{m}$  thick and is composed primarily of Si oxides and  $\text{TiNb}_2\text{O}_7$ . Comparing the oxide scales of the 4Zr and 8Zr alloys reveals that the latter exhibits a more obvious layered structure, with increased content and size of  $\text{ZrO}_2$ . This demonstrates that whether the oxide scale becomes layered and whether  $\text{ZrO}_2$  forms depend on the Zr content in the alloy. Higher Zr content indeed promotes selective oxidation of Ti during oxidation, forming a dense outer oxide layer that inhibits further inward oxygen diffusion and effectively improves oxidation resistance. Lee and Woo [29] also found that Zr can promote the formation of other oxides and nitrides, thereby modifying the oxidation resistance of TiAl-W alloys.

The oxide scale composition and microstructure of the 0Zr, 2Zr, and 8Zr alloys show no obvious difference after short oxidation times (1 and 5 h). However, when the oxidation time extends to 50 h, significant differences appear in scale-substrate adhesion, scale thickness, and structure among the three alloys, indicating that the effect of Zr on the oxidation resistance of Nb-Ti-Si base ultrahigh-temperature alloys becomes more pronounced in the later oxidation stages.

---

## Conclusions

- (1) In the as-cast state, Nb-22Ti-15Si-5Cr-3Hf-3Al-xZr ( $x = 0, 0.5, 1, 2, 4, 8$ ) alloys all consist of  $\gamma\text{-(Nb, X)}_5\text{Si}_3$  and Nbss phases. With increasing Zr content, the amount of primary  $\gamma\text{-(Nb, X)}_5\text{Si}_3$  increases and its size becomes larger. Zr shows a strong tendency for solid solution, primarily dissolving in the silicide phase by substituting for Nb atoms.
- (2) The oxidation kinetics curves of alloys with different Zr contents at 1250  $^\circ\text{C}$  follow a parabolic law. Zr addition improves the oxidation resistance of Nb-Ti-Si base alloys and reduces the oxidation rate because it promotes

the formation of stable oxidation products  $\text{TiNb}_2\text{O}_7$  and  $\text{TiO}_2$  while decreasing the content of  $\text{Nb}_2\text{O}_5$  and  $\text{Ti}_2\text{Nb}_{10}\text{O}_{29}$  in the oxide scale, thereby improving scale compactness.

- (3) After oxidation at 1250 °C for 50 h, the oxide scales on the 4Zr and 8Zr alloys did not spall and exhibited a layered structure: the outermost layer is a dense single-phase  $\text{TiO}_2$  layer, the middle layer consists mainly of  $\text{ZrO}_2$ ,  $\text{TiO}_2$ , and  $\text{TiNb}_2\text{O}_7$ , and the inner layer is composed primarily of Si oxides and  $\text{TiNb}_2\text{O}_7$ , with the scale remaining intact and well-bonded to the substrate.

---

## References

- [1] Bewlay B P, Jackson M R, Lipsitt H A. *Metall Mater Trans*, 1996; 27A: 3801
- [2] Grammenos I, Tsakirooulos P. *Intermetallics*, 2010; 18: 242
- [3] Bewlay B P, Jackson M R, Zhao J C, Subramanian P R. *Metall Mater Trans*, 2003; 34A: 2043
- [4] Wu C L, Zhou L Z, Guo J T. *Acta Metall Sin*, 2006; 42: 1061 (伍春兰, 周兰章, 郭建亭. *金属学报*, 2006; 42: 1061)
- [5] Kang Y W, Qu S Y, Song J X, Han Y F. *Acta Metall Sin*, 2008; 44: 593 (康永旺, 曲士昱, 宋尽霞, 韩雅芳. *金属学报*, 2008; 44: 593)
- [6] Jia L N, Gao M, Ge J R, Zheng L J, Sha J B, Zhang H. *Acta Metall Sin*, 2011; 47: 88 (贾丽娜, 高明, 盖京茹, 郑立静, 沙江波, 张虎. *金属学报*, 2011; 47: 88)
- [7] Wang J, Guo X P, Guo J M. *Chin J Aeronaut*, 2009; 22: 544
- [8] Zhang S, Guo X P. *Intermetallics*, 2015; 57: 83
- [9] Xiong B W, Cai C C, Wan H, Zheng Y H. *J Alloys Compd*, 2009; 486: 330
- [10] Guo J M, Guo X P, Song S G. *Acta Metall Sin*, 2008; 44: 574 (郭金明, 郭喜平, 宋曙光. *金属学报*, 2008; 44: 574)
- [11] Zelenitsas K, Tsakirooulos P. *Mater Sci Eng*, 2006; A416: 269
- [12] Geng J, Tsakirooulos P, Shao G S. *Mater Sci Eng*, 2006; A441: 1
- [13] Li Z F, Tsakirooulos P. *Intermetallics*, 2012; 26: 18
- [14] Wang L G, Jia L N, Cui R J, Zheng L J, Zhang H. *Chin J Aeronaut*, 2012; 25: 292
- [15] Grammenos I, Tsakirooulos P. *Intermetallics*, 2011; 19: 1612
- [16] Geng J, Tsakirooulos P. *Intermetallics*, 2007; 15: 382
- [17] Behrani V, Thom A J, Kramer M J, Akinc M. *Intermetallics*, 2006; 14: 24
- [18] Vellios N, Tsakirooulos P. *Intermetallics*, 2010; 18: 1729
- [19] Vellios N, Tsakirooulos P. *Intermetallics*, 2007; 15: 1518
- [20] Yuan W H, Liang Z Y. *Mater Des*, 2011; 32: 4195
- [21] Mousa M, Wanderka N, Timpel M, Singh S, Krüger M, Heilmaier M, Banhart J. *Ultramicroscopy*, 2011; 111: 706
- [22] Gorr B, Wang L, Burk S, Azim M, Majumdar S, Christ H J, Mukherji D, Rösler J, Schliephake D, Heilmaier M. *Intermetallics*, 2014; 48: 34
- [23] Yu Q H, Zhou C G, Zhang H Y, Zhao F. *J Eur Ceram Soc*, 2010; 30: 889
- [24] Li X, Guo X P, Qiao Y Q. *Oxid Met*, 2015; 83: 253

- [25] Li X, Guo X P. Acta Metall Sin, 2012; 48: 1394 (李轩, 郭喜平. 金属学报, 2012; 48: 1394)
- [26] Tian Y X, Guo J T, Sheng L Y, Cheng G M, Zhou L Z, He L L, Ye H Q. Intermetallics, 2008; 16: 807
- [27] Li X F, Guo X P. Acta Metall Sin, 2013; 49: 853 (李小飞, 郭喜平. 金属学报, 2013; 49: 853)
- [28] Liu A Q, Sun L, Li S S, Han Y F. J Rare Earth, 2007; 25: 474
- [29] Lee D B, Woo S W. Intermetallics, 2005; 13: 169

*Note: Figure translations are in progress. See original paper for figures.*

*Source: ChinaXiv — Machine translation. Verify with original.*